catalysts

MDPI

Article

The Influence of Pluronic F-127 Modification on Nano Zero-Valent Iron (NZVI): Sedimentation and Reactivity with 2,4-Dichlorophenol in Water Using Response Surface Methodology

Yajun Li, Yongxiang Zhang *, Qi Jing and Yuhui Lin

Beijing University of Technology, 100 Ping Le Yuan, Chaoyang District, Beijing 10024, China; liyjbjut@emails.bjut.edu.cn (Y.L.); jingqi@bjut.edu.cn (Q.J.); S201904283@emails.bjut.edu.cn (Y.L.)

* Correspondence: yxzhang@bjut.edu.cn; Tel.: +86-139-1082-1850

Received: 23 February 2020; Accepted: 2 April 2020; Published: 8 April 2020

Abstract: Nano zero-valent iron (NZVI) is widely used for reducing chlorinated organic pollutants in water. However, the stability of the particles will affect the removal rate of the contaminant. In order to enhance the stability of nano zero-valent iron (NZVI), the particles were modified with F-127 as an environmentally friendly organic stabilizer. The study investigated the effect of the F-127 mass ratio on the colloidal stability of NZVI. Results show that the sedimentation behavior of F-NZVI varied at different mass ratios. A biphasic model was used to describe the two time-dependent settling processes (rapid sedimentation followed by slower settling), and the settling rates were calculated. The surface morphology of the synthesized F-NZVI was observed with a scanning electron microscope (SEM), and the functional groups of the samples were analyzed with Fourier Transform Infrared Spectroscopy (FTIR). Results show that the F-127 was successfully coated on the surface of the NZVI, and that significantly improved the stability of NZVI. Finally, in order to optimize the removal rate of 2,4-dichlorophenol (2,4-DCP) by F-NZVI, three variables were tested: the initial concentration 2,4-DCP, the pH, and the F-NZVI dosage. These were evaluated with a Box-Behnken Design (BBD) of response surface methodology (RSM). The experiments were designed by Design Expert software, and the regression model of fitting quadratic model was established. The following optimum removal conditions were determined: pH = 5, 3.5 g·L^{-1} F-NZVI for 22.5 mg·L^{-1} of 2,4-DCP.

Keywords: pluronic F-127; nano zero-valent iron; sedimentation; 2,4-dichlorophenol; response surface methodology

1. Introduction

Chlorophenols (CPs) are widely used in wood preservatives, pesticides, lubricants, dyestuffs, and the synthesis of other chemicals [1–3]. At present, CPs have raised great concern in the protection of human health, due to their high toxicity and long persistence in the environment [4,5]. 2,4-dichlorophenol (2,4-DCP), as a long-lived pollutant, is one of the representative phenolic compounds and a key intermediate in the synthesis of chloride-based herbicides. It has been listed as a priority pollutant by the U.S. Environmental Protection Agency (EPA) (2003) [6,7]. Removal methods of 2,4-DCP from water have become important in the environment field.

Over the past years, nano zero-valent iron (NZVI) has been reported to be a promising nanomaterial for the treatment of chlorinated phenols in wastewater, drinking water, and groundwater because of its large specific surface area, excellent adsorption, low redox potentials, small particle size, and high reaction activity [8–11]. In fact, the NZVI is applied for the removal of various pollutants in water, such as dye, antibiotics, chlorophenols, organic pollutants, and heavy metals [12–14]. However, there

are still some technical challenges that hinder their large-scale practical applications. On one hand, the tendency of bare NZVI particles to agglomerate into large particles, due to the van der waals interactions and magnetic attraction forces, leads to a considerable decrease in their dispersibility and mobility. On the other hand, bare NZVI particles are easy to oxidize, which reduces their reductive activity, durability, and efficiency [15,16].

In order to address these drawbacks, researchers have attempted to stabilize and disperse NZVI particles with the following method: 1) offering a support for NZVI particles, such as kaolinite [17], bentonite [18], activated carbon [19,20], mesoporous carbon [21], and mesoporous silica [22]; 2) changing the surface properties of NZVI with surfactant [23], polyelectrolyte, or nature biopolymer [24]. Most solid supports cannot be used to control stability and nanometer distribution of the NZVI particles. In addition, the method of solid support is complex and the price is relatively expensive. Unlike solid supports, surface modification can stabilize the NZVI particles by controlling the interaction between them. This study aims to provide a modifier that is easily used in the environment and which can increase the colloidal stability of the NZVI in water. Pluronic F-127, made up of hydrophilic groups (PEOs) and hydrophobic groups (PPOs), is a kind of water-soluble amphiphilic copolymer which can self-assemble in an aqueous solution and has a less adverse effect. When released to the environment, F-127 can be degraded by natural microorganisms [25].

Response surface methodology (RSM) is a mathematical and statistical approach for optimizing and estimating the interaction between various influencing factors with a limited number of experiments [26]. In recent years, RSM has been used to design experiments in various fields [27–29].

In this work, we selected F-127 to modify the NZVI with different mass ratios (F-NZVI (F-127/Fe, m/m)). The sedimentation experiments of F-NZVI particles focused on the effect of F-127 on NZVI stability, and the synthesized particles were characterized with a scanning electron microscope (SEM) and Fourier Transform Infrared Spectroscopy (FTIR). In order to obtain the optimum conditions for the experimental design, the initial concentration of 2,4-DCP, the pH, and the F-NZVI dosage were evaluated by RSM with Box-Behnken Design (BBD). 2.4-DCP was chosen as a model organic pollutant, and the removal rate of 2,4-DCP was evaluated as a response value.

2. Results and Discussion

2.1. Structure and Performance of F-NZVI (F-127/Fe, m/m)

2.1.1. Morphology of NZVI and F-NZVI

The SEM images of F-NZVI are depicted in Figure 1. It could be observed that the F-NZVI particles were spherical and organized in a chain-like structure. The spherical form of F-NZVI suggests that numerous reactive sites could be provided with a chain-like structure, due to the magnetic interactions between the F-NZVI particles, which could be maintained in a stable state [30]. The diameters of F-NZVI (m/m, 2:1) range from 70 to 80 nm. The shape and diameter of the bare NZVI was irregular in previous research [31]. Compared with bare NZVI, F-NZVI shows a significantly increased dispersity. Obviously, F-127 as a modifier can increase the dispersity of NZVI.

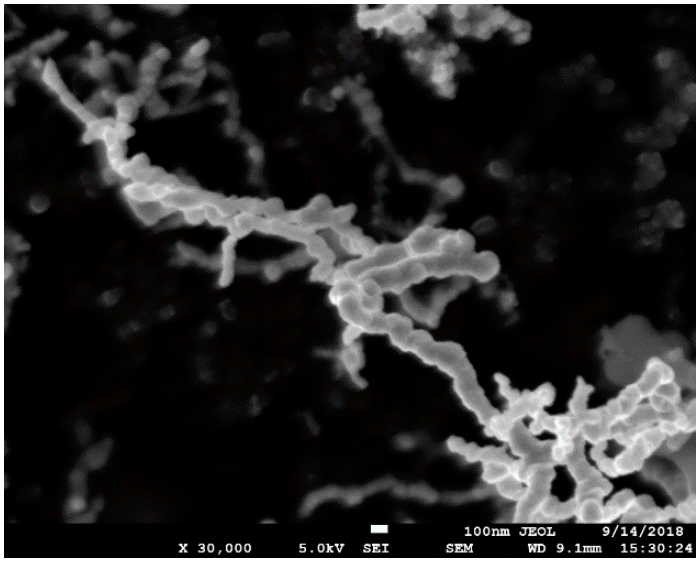

Figure 1. SEM micrographs of F-NZVI (2:1).

2.1.2. FTIR Analysis

Figure 2 refers to the FTIR spectra of NZVI, F-127, and F-NZVI, respectively. The presence of O–H at 3430 and 1633 cm^{-1} indicates that some hydroxyl groups existed on the surface of F-127, NZVI, and F-NZVI samples [32]. The FTIR bands in the F-127 spectra have peaks at 2899 cm^{-1}, which could be attributed to the stretching –CH from the alkyl groups, and a strong band ranging from 1100 to 1150 cm^{-1} refers to C–O [33]. The stretching bands at 1360 and 1472 cm^{-1} confirms asymmetric and symmetric stretching of CH_3 groups, respectively [34]. The results correspond to the molecular formula of F-127. In the FTIR spectra of NZVI, the peak at 669 cm^{-1} relates to the partial oxidation loaded on the NZVI and confirms that NZVI was partly oxidized [35]. Changes between the adsorption peaks of F-NZVI and the FTIR spectra of NZVI were observed. For example, the peaks at 1132 and 1440 cm^{-1} were significantly increased and the Fe–O vibrations were significantly reduced. The results demonstrate that F-127 was combined firmly with the NZVI.

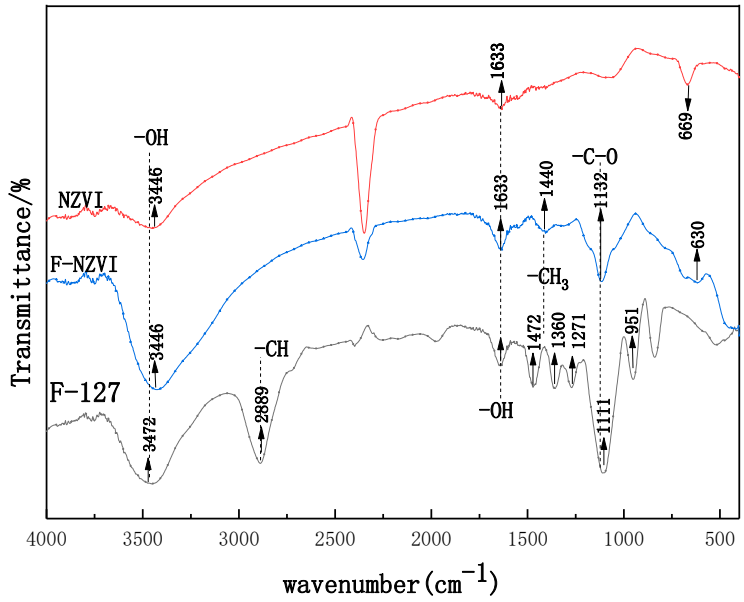

Figure 2. FTIR micrographs of F-127, NZVI, and F-NZVI (2:1).

2.2. Sedimentation test of F-NZVI Particles with Different Mass Ratios

The colloidal stabilities of F-NZVI suspensions with different mass ratios were investigated by measuring the sedimentation kinetics of F-NZVI dispersions (Figure 3). As shown in Figure 3, the downward trend of the relative concentration of F-NZVI can be divided into a two-stage process: at the beginning, an obviously rapid settling of F-NZVI particles; then, a much slower settling. The biphasic model was used to describe the two-stage process and expressed as Equation (1) [36]:

$$C/C_0 = P_{rapid}\ (e^{-kr \times t}) + P_{slow}\ (e^{-ks \times t}) \quad (1)$$

where C is the concentration of F-NZVI at time t and C_0 is the initial concentration of F-NZVI at t = 0; P_{rapid} and P_{slow} are the settling compartments; kr and ks are the settling rate constants for the compartments (s^{-1}); and t is time (s).

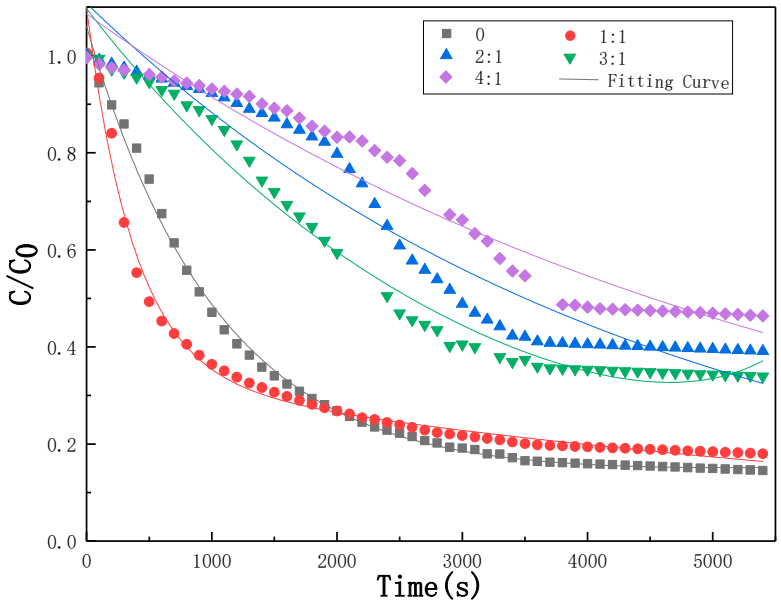

Figure 3. Settlement curves of F-NZVI at different mass ratios.

The fitting curves of F-NZVI with different mass ratios are presented in Figure 3. They indicate that the experimental data were well-fitted to the biphasic model, with the square of the correlation coefficient of the linear regression (R^2) > 0.9. The calculated results, according to the biphasic rate model, are shown in Table 1. The results indicate that the colloidal stability of NZVI can be significantly improved by F-127 at a suitable mass ratio. Significant and rapid sedimentation of the NZVI and F-NZVI (m/m, 1:1) are observed at the outset of the experiment. From 0 to 2000 s, the settling rate of F-NZVI (m/m, 1:1) is faster than NZVI. F-127 can self-assemble to micelle in water and form a core-shell structure, and this can affect the core-shell structure of NZVI. When the mass ratio of F-NZVI is 1:1 (m/m), the particle has a thin shell. Van der Waals forces inside the nuclear shell affect the repulsion force coming from the outside, making the particles less stable in water. The downturn of the settlement curve of F-NZVI (m/m, 2:1) is gentle. After 1 h, the relative concentration of F-NZVI (m/m, 2:1) is 0.39, and the concentration of F-NZVI (m/m, 2:1) is 0.39 g·L^{-1}. The colloidal stability of NZVI (m/m, 2:1) is good. The downturn of the settlement curve of F-NZVI (m/m, 4:1) is the same as F-NZVI (m/m, 2:1). The relative concentration of F-NZVI (m/m, 4:1) is stable at around 0.46, and the concentration of F-NZVI (m/m, 4:1) is 0.46 g·L^{-1}. The colloidal stability is best when the core-shell structure of F-NZVI has mass ratios of 2:1 and 4:1, lipophilic groups inside the core shell structure, and hydrophilic groups with negative charge outside the core shell structure.The repulsive forces between F-NZVI particles, caused by hydrophilic groups and the steric barrier effect, strengthens the stability of NZVI.

Table 1. Settling rate constants (k) and settled fractions (F) in the rapid and slow compartments of particle sedimentation, calculated from the biphasic rate model ($R^2 > 0.9$).

Mass Ratio	P_{rapid} (%)	K_{rapid} (s^{-1})	P_{slow} (%)	K_{slow} (s^{-1})	R^2	R^2_{adj}
0	0.94	0.0009	0.11	−0.00005	0.99	0.99
1:1	0.76	0.0026	0.34	0.0001	0.99	0.99
2:1	0.55	0.0002	0.55	0.0002	0.93	0.93
3:1	1	0.0003	0.002	−0.0012	0.98	0.98
4:1	0.54	0.0001	0.54	0.0001	0.93	0.93

Zeta potential is a key index of the stability of NZVI and a higher absolute value indicates more stability [37]. Zeta potentials of F-NZVI with different mass ratios are listed in Table 2. The results indicate that F-127 can change the surface charge of NZVI from positive to negative, suggesting interactions between the positively charged NZVI and the negatively charged F-127. The distinctions of zeta potentials between NZVI and F-NZVI indicate that F-127 was successfully coated on the surface of NZVI. The dispersion of the F-NZVI particles could be attributed to the adsorption of F-127 on the surface of the NZVI particles, which increases the electrostatic repulsion effect. Additionally, it was interesting to observe that the negative charge of F-NZVI changed when the mass ratios of F-NZVI increased from 0 to 3:1, while it decreased to some degree. As the mass ratio increased to 4:1, the zeta potential decreased. The nanoparticles were more stable, since steric effect impeded the release of a negative charge. This indicates that a steric effect also played an important role in stabilizing the F-NZVI particles.

Table 2. Zeta potential (mV) for F-NZVI with different mass ratios.

F-NZVI (F-127/NZVI, m/m)	0	1:1	2:1	3:1	4:1
Zeta potential (mV)	4.52	−10.45	−18.39	−21.4	−12.4

F-127 plays a significant effect on the aggregation and colloidal stability of F-NZVI. The mass ratio of 2:1 is better, and the mass ratio of 4:1 is the best. Combined with the zeta potentials of F-NZVI, we adopted the F-NZVI (m/m, 2:1) for the following test.

2.3. Analysis of 2,4-DCP Removal by RSM

2.3.1. 2,4-DCP Removal Rate Response Model and Variance Analysis

Table 3 lists a total of 17 experimental runs and the corresponding results. The experimental runs, with a different combination of three factors, aim to investigate the effects of these factors on the 2,4-DCP removal rate (V). According to the RSM analysis, a quadratic polynomial equation, which expressed the relationship between the removal rate of 2,4-DCP and the independent variables, was established to obtain the predicted values of response. The model, in accordance with actual factors, is shown as Equation (2).

$$V\ (\%) = -3.53 + 0.85A + 16.8B + 15.8 \times C + 0.02 \times AB - 0.05 \times BC - 0.113 \times AC - 0.02 \times A^2 - 1.92425 \times B^2 - 1.55 \times C^2 \quad (2)$$

Table 4 presents the results of analysis of variance (ANOVA) for the response surface quadratic model. F-value evaluates the statistical significance of modelling, and P-value determines the significance of factors for the response. Generally, a relatively large F-value and small P-value are significant. Therefore, the model is significant, due to the F-value (3482.27) and P-value (less than 0.0500). The Lack of Fit F-value of 3.93 implies the error is not significant, relative to the pure error. The R^2 value of 0.9998 and the adjusted R^2 value of 0.9995 in the quadratic model imply the veracity and suitability of the model. The predicted R^2 value of 0.9972 is in reasonable agreement with the adjusted

R^2 value of 0.9995. Furthermore, the relatively low value of coefficient of variation (CV% = 0.41%) suggests that this model improved the precision and reliability of the tests. The P-value of AB, AC, and BC are 0.0003, <0.0001, and 0.0026, respectively, which means that these model terms are significant.

Table 3. Response surface experiment design and results.

Test	Concentration of 2,4-DCP (mg/L)	pH	F-NZVI Dosage (g/L)	Experiment V (%)	Predicted V (%)
1	5	5	1	50.1	50.02
2	5	3	3.5	67.67	67.85
3	5	7	3.5	56.8	56.97
4	5	5	6	71.15	70.88
5	22.5	3	1	50.8	50.70
6	22.5	3	6	68.31	68.41
7	22.5	5	3.5	72.1	72.29
8	22.5	5	3.5	72.15	72.29
9	22.5	5	3.5	72.32	72.29
10	22.5	5	3.5	72.42	72.29
11	22.5	5	3.5	72.48	72.29
12	22.5	7	1	42.7	42.60
13	22.5	7	6	57.95	58.05
14	40	3	3.5	55.9	55.73
15	40	5	1	43.55	43.82
16	40	5	6	56.05	56.13
17	40	7	3.5	48.32	48.14

Table 4. ANOVA of 2,4-DCP yield.

Source	Sum of Squares	Degree of Freedom	Mean Square	F-Value	P-Value	
Model	1936.59	9	215.18	3482.27	<0.0001	Significant
the initial concentration of 2,4-DCP (mg/L)	219.45	1	219.45	3551.44	<0.0001	-
pH	170.29	1	170.29	2755.91	<0.0001	-
F-NZVI dosage(g/L)	549.63	1	549.63	8894.77	<0.0001	-
AB	2.71	1	2.71	43.79	0.0003	-
AC	18.28	1	18.28	295.76	<0.0001	-
BC	1.28	1	1.28	20.66	0.0026	-
A^2	232.1	1	232.1	3756.1	<0.0001	-
B^2	249.45	1	249.45	4036.88	<0.0001	-
C^2	392.66	1	392.66	6354.59	<0.0001	-
Residual	0.43	7	0.062	-	-	-
Lack of Fit	0.32	3	0.11	3.93	0.1095	Not Significant
Pure Error	0.11	4	0.027	-	-	-
Cor Total	1937.03	16	-	-	-	-

R^2 = 0.9998, R^2_{adj} = 0.9995.

As a result, the established model is proved to be highly accurate in the prediction of values in the 2,4-DCP removal test.

2.3.2. Quantitative Effects of the Factors

A three-dimensional contour map presents the relationships among the two independent variables and the removal rate of 2,4-DCP. Figure 4 shows the change regulation of the V value under the effects of two independent variables.

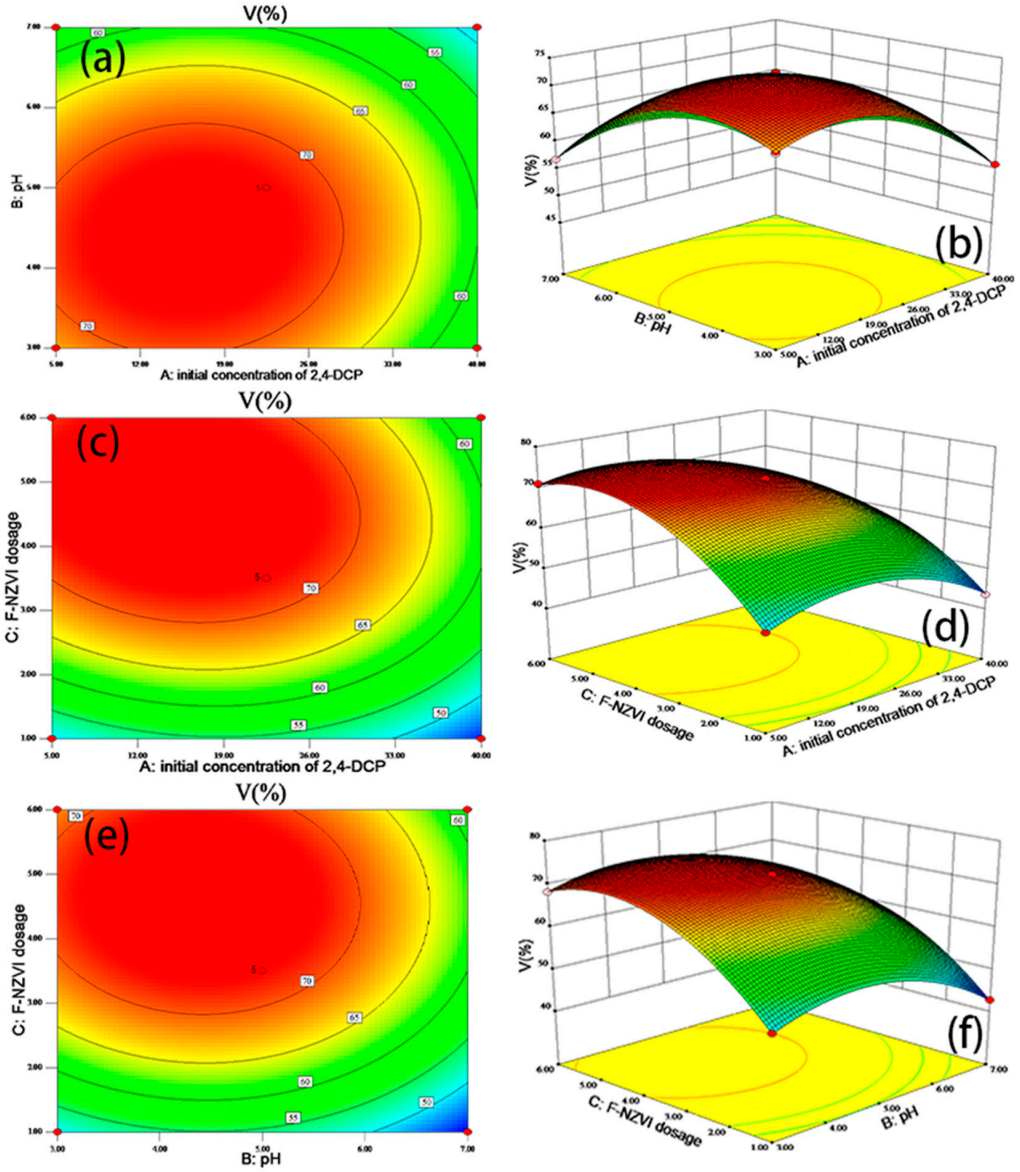

Figure 4. 2D contour and 3D response surface plots for the interactive effect of (**a**,**b**) the initial concentration of 2,4-DCP and the pH, (**c**,**d**) the initial concentration of 2,4-DCP and the F-NZVI dosage, (**e**,**f**) the pH and the F-NZVI dosage on the removal rate(V) of 2,4-DCP.

As demonstrated in Figure 4a,b, the value of V gradually increases to the peak value as the initial concentration of 2,4-DCP increases from 5 to 22.5 mg/L, and, then, descends as A continuously increases. Meanwhile, the V value reaches the peak value with pH (B) of 5 and also displays a decrease as B continuously increases. The V value reaches the maximum value when A = 22.5 mg/L and B = 5. A suitable concentration of 2,4-DCP or pH facilitates the removal rate of 2,4-DCP. High or low A or B values may decrease the removal rate of 2,4-DCP.

Figure 4c,d shows the interaction between the initial concentration of 2,4-DCP and F-NZVI dosages on the removal rate of 2,4-DCP. The V value gradually reaches the peak value with a moderate F-NZVI dosage, and decreases as C increases. Obviously, when increasing the initial concentration of 2,4-DCP within an appropriate range, the removal rate improves. V reaches the maximum value when A = 22.5 mg/L and C = 3.5 g/L. However, excess F-NZVI dosages would lead to a decline of the efficiency of the 2,4-DCP removal rate because excess F-NZVI dosages may affect dispersion and the molecules of 2,4-DCP cannot migrate to the iron surface.

Figure 4e,f shows the interaction between pH and F-NZVI dosages on the efficiency of the 2,4-DCP removal rate. It is clear that as the pH and F-NZVI dosages increase, the efficiency of the 2,4-DCP removal rate increases and, then, starts to slightly decrease. The V value reaches the maximum value with a moderate B value of 5 and a C value of 3.5 g/L. The passivation layer formed on the surface of F-NZVI, with a high pH, hinders electron transfer from highly active zero-valent iron cores. Hence, the removal rate of 2,4-DCP is reduced.

In short, A, B, and C are key points of variables that affect the removal rate of 2,4-DCP on account of the P-value of <0.05. The results also show that A, B, and C significantly affect the removal rate of 2,4-DCP as a single independent factor, which is consistent with the results of the ANOVA.

3. Materials and Methods

3.1. Chemicals and Materials

The pluronic F-127 ($EO_{106}PO_{70}EO_{106,}$) used in this study was purchased from Shanghai Macklin Biochemical Co., Ltd. (Shanghai, China). Ferrous sulfate ($FeSO_4{\cdot}7H_2O$, AR), sodium borohydride ($NaBH_4$, AR), nickelous sulfate ($NiSO_4{\cdot}6H_2O$, AR), 2,4-dichlorophenol (2,4-DCP, AR), 2-chlorophenol (2-CP, AR), 4-chlorophenol (4-CP, AR), and phenol (AR) were obtained from Tianjin Fuchen Chemical Reagent Factory (Tianjin, China). Solutions containing 2,4-DCP, 2-CP, 4-CP, and phenol were prepared with distilled water to the desired concentration and retained in the brown volumetric for further use. All solutions were prepared with distilled water. All chemicals were used without further purification.

3.2. Preparation and Characterization of Bare NZVI and F-NZVI Particles

F-NZVI particles with different mass ratios of F-127/NZVI were prepared by a liquid phase reducing method with ferrous iron and sodium borohydride in an N_2 atmosphere. The chemistry reaction experiments were put into a 1000 mL three-necked round-bottomed flask, in which the middle neck was connected to the agitator, the second neck was connected to N_2 gas, and the third neck was connected to $NaBH_4$ solution. Take the F-NZVI samples with 2:1(m/m) F-127/NZVI as an example. Firstly, 1 g F-127 was placed in 250 mL ultrapure water in a 1000 mL three-necked flask at room temperature. It was stirred mechanically (250 r/min) for 25 min, before 2.484 g ferrous sulfate was added to the F-127 solution. The mixture solution was continuously stirred (250 r/min) for 15 min. Subsequently, a freshly prepared $NaBH_4$ solution (0.678 g $NaBH_4$ in 250 mL ultrapure water) was added drop-wise (5 mL/min) into the mixture solution of F-127 and Ferrous sulfate, and stirred constantly at 250 r/min under a N_2 atmosphere. The solution was stirred (250 r/min) for another 30 min until the $NaBH_4$ solution was fully incorporated into the mixture solution. The black particles were produced, and the solution turned black. Afterwards, the F-NZVI particles were collected by vacuum filtration and washed three times with ultrapure water and anhydrous ethanol. Finally, the fresh F-NZVI was dried by Freeze Drier (FD-1 A-50) and kept in a sealed bottle, prior to use. (Equation (3)) [31]:

$$Fe^{2+} + 6H_2O + 2BH_4^- \rightarrow Fe^0 \downarrow + 2B(OH)_3 + 7H_2 \uparrow \quad (3)$$

The pristine NZVI was prepared, following the method as described above, except no F-127 was added in this experiment.

Using a C-18 column, the concentrations of 2,4-DCP, 2-CP, 4-CP, and phenol in the liquor were measured by high performance liquid chromatography (LC-2030C, Shimadzu (China), Beijing branch, Chaoyang District, Beijing 100020 P.R. China). The surface morphology of F-NZVI particles was characterized with SEM (JSM-7610F-Plus, JEOL Ltd., Akishima, Tokyo, Japan). The functional groups on the surface of F-127, NZVI, and F-NZVI were obtained using FTIR (IRAffinity-1S, Shimadzu (China), Beijing branch, Chaoyang District, Beijing 100020 P.R. China) and chemical bonding of the samples over a spectral range of 400–4000 cm^{-1}.

3.3. Stability Study of F-NZVI Particles with Different Mass Ratios

The colloidal stabilities of F-NZVI particles were evaluated by measuring the sedimentation kinetics of F-NZVI particles and the zeta potential at different mass ratios (F-127/NZVI:0, 1:1, 2:1, 3:1, 4:1). In the sedimentation experiments, the concentration of F-NZVI particles was 1 g L^{-1}. F-NZVI suspensions with different mass ratios were sonicated for 10 min, and a 1 ml F-NZVI suspension was transferred to a glass cuvette for spectrophotometric analysis. The sedimentation of F-NZVI was measured by monitoring the optical absorbance at 508 nm by UV-vis spectrophotometry in intervals for 100 min. The measurements were carried out at room temperature (27 °C), and all the experiments were run in duplicates or triplicates. Surface charges of F-NZVI with different mass ratios were measured with a zeta potential analyzer (90 Plus Zeta, Brookhaven Instruments, Holtsville, NY, America).

3.4. RSM Experimental Design

The RSM is extensively used for evaluating the relationship between a combination of experimental factors and response values, using multiple regression equations. It aims to find the optimum removal conditions. The removal experiments were designed by the Design Expert software (8.0.6, Stat-Ease, Inc., Minneapolis, MN, America) to formulate optimization of the experimental factors. The effect of three independent experimental variables on the removal rate of V (response value) was developed by BBD at three levels: the initial concentration of 2,4-DCP (mg L^{-1}, (A)), pH (B), and the F-NZVI dosage (g L^{-1}, (C)). Table 3 presents the level of experimental variables and experimental orders. The sum of 17 operational variables from the study was applied toward the construction of a quadratic model. After experiments were completed, a second order polynomial model has been expressed as Equation (4):

$$V = \alpha_0 + \alpha_1 A + \alpha_2 B + \alpha_3 C + \alpha_{12} AB + \alpha_{13} AC + \alpha_{23} BC + \alpha_{11} A^2 + \alpha_{22} B^2 + \alpha_{33} C^2 \quad (4)$$

where V refers to the removal rate of 2,4-DCP; A, B, and C are independent variables (the initial concentration of 2,4-DCP, the pH, and the F-NZVI dosage, respectively); α_0 is the constant coefficient; α_1, α_2, and α_3 are linear coefficients; α_{11}, α_{22}, and α_{33} are quadratic coefficients; finally, α_{12}, α_{13} and α_{23} are interaction coefficients.

Table 5 displays the parameters, and we assess the fit quality of the polynomial model equation by the coefficient of determination R^2 and adjusted R^2. Model terms are chosen or rejected depending on the probability of P value with a 95% confidence level. 3D surface plots not only visualize the relationship between the removal rate and experimental factors utilized in the design but also determine the optimum condition, based on the main parameters.

Table 5. Levels of factors and variables used for optimization.

Factors	Symbol	Coded Levels		
-	-	−1	0	1
initial concentration of 2,4-DCP (mg L^{-1})	A	5	22.5	40
pH	B	3	5	7
F-NZVI dosage (g L^{-1})	C	1	3.50	6

4. Conclusions

In this work, F-127 was developed to modify the NZVI, and it was found that F-127 significantly increased the stability of NZVI. SEM analysis indicated that F-127, as a modifier, can enhance the dispersity of NZVI. Compared with the traditional NZVI, F-NZVI had better stability. Zeta potential and FTIR analysis indicated that F-127 played a significant effect on the aggregation and sedimentation behavior of F-NZVI. The sedimentation tests indicated that there is a two-stage process (rapid sedimentation and slow suspension) of F-NZVI in water. F-127 had an important effect on electrostatic

repulsion and the steric effect that makes F-NZVI stable. The experimental conditions were optimized through RSM. The maximal removal rate of 72.29% was obtained under optimal operational conditions, with a pH of 5, F-NZVI dosage of 3.5 g/L, and an initial 2,4-DCP concentration of 22.5 mg/L.

Author Contributions: Conceptualization, Y.Z.; Formal analysis, Y.L. (Yajun Li); Investigation, Y.L. (Yajun Li) and Y.L. (Yuhui Lin); Methodology, Y.L. (Yajun Li); Project administration, Y.Z.; Resources, Y.Z.; Supervision, Y.Z.; Writing—Original draft, Y.L. (Yajun Li); Writing—Review & editing, Y.L. (Yajun Li), Y.Z. and Q.J. All authors have read and agreed to the published version of the manuscript.

Funding: This research received no external funding.

Acknowledgments: This work was supported by the National Key Research and Development Program of China under No.2016YFC0401404.

Conflicts of Interest: The authors declare no conflicts of interest.

References

1. Munoz, M.; de Pedro, Z.M.; Casas, J.A.; Rodriguez, J.J. Improved wet peroxide oxidation strategies for the treatment of chlorophenols. *Chem. Eng. J.* **2013**, *228*, 646–654. [CrossRef]
2. Li, J.J.; Li, X.; Yang, R.; Qu, L.B. A sensitive electrochemical chlorophenols sensor based on nanocomposite of ZnSe quantum dots and cetyltrimethylammonium bromide. *Anal. Chim. Actal.* **2013**, *804*, 76–83. [CrossRef]
3. Han, L.J.; Zhang, H.W.; Liu, D.; Song, J.L.; Chuan, G.K.; Jaenicke, S. Efficient photodegradation of chlorophenols by BiOBr/$NaBiO_3$ heterojunctioned composites under visible light. *J. Hazard. Mater.* **2018**, *341*, 83–92. [CrossRef] [PubMed]
4. Xiong, J.; Ma, Y.; Yang, W.; Zhong, L.S. Rapid, highly efficient and stable catalytic hydrodechlorination of chlorophenols over novel Pd/CNTs-Ni foam composite catalyst in continuous-flow. *J. Hazard. Mater.* **2018**, *355*, 89–95. [CrossRef] [PubMed]
5. Long, G.; Ding, J.; Xie, L.; Sun, R.; Chen, M.; Zhou, Y.; Huang, X.; Han, G.; Li, Y.; Zhao, W. Fabrication of mediator-free g-C_3N_4/Bi_2WO_6 Z-scheme with enhanced photocatalytic reduction dechlorination performance of 2,4-DCP. *Appl. Surf. Sci.* **2018**, *455*, 1010–1018. [CrossRef]
6. Ruan, X.; Liu, H.; Wang, J.W.; Zhao, D.Y.; Fan, X.Y. A new insight into the main mechanism of 2,4-dichlorophenol dechlorination by Fe/Ni nanoparticles. *Sci. Total Environ.* **2019**, *697*, 133996. [CrossRef]
7. Quan, X.C.; Shi, H.; Liu, H.; Lv, P.P.; Qian, Y. Enhancement of 2,4-dichlorophenol degradation in conventional activated sludge systems bioaugmented with mixed special culture. *Water Res.* **2004**, *38*, 245–253. [CrossRef]
8. Su, Y.M.; Adeleye, A.S.; Huang, Y.X.; Sun, X.Y.; Dai, C.M.; Zhou, X.F.; Zhang, Y.L.; Keller, A.A. Simultaneous removal of cadmium and nitrate in aqueous media by nanoscale zerovalent iron (nZVI) and Au doped nZVI particles. *Water Res.* **2014**, *63*, 102–111. [CrossRef]
9. Li, B.; Zhu, J. Removal of p-chloronitrobenzene from groundwater: Effectiveness and degradation mechanism of a heterogeneous nanoparticulate zero-valent iron (NZVI)-induced Fenton process. *Chem. Eng. J.* **2014**, *255*, 225–232. [CrossRef]
10. Fu, F.L.; Dionysiou, D.D.; Liu, H. The use of zero-valent iron for groundwater remediation and wastewater treatment: A review. *J. Hazard. Mater.* **2014**, *267*, 194–205. [CrossRef]
11. Simeonidis, K.; Mourdikoudis, S.; Kaprara, E.; Mitrakas, M.; Polavarapu, L. Inorganic engineered nanoparticles in drinking water treatment: A critical review. *Environ. Sci. Water Res. Technol.* **2016**, *2*, 43–70. [CrossRef]
12. Liu, J.; Liu, A.R.; Wang, W.; Li, R.F.; Zhang, W.X. Feasibility of nanoscale zero-valent iron (nZVI) for enhanced biological treatment of organic dyes. *Chemosphere* **2019**, *237*, 124470. [CrossRef] [PubMed]
13. Ma, J.Y.; Gu, J.; Wang, X.J.; Peng, H.L.; Wang, Q.Z.; Zhang, R.R.; Hu, T.; Bao, J.F. Effects of nano-zerovalent iron on antibiotic resistance genes during the anaerobic digestion of cattle manure. *Bioresour. Technol.* **2019**, *289*, 121688. [CrossRef]
14. Kaifas, D.; Malleret, L.; Kumar, N.; Fétimi, W.; Claeys-Bruno, M.; Sergent, M.; Doumenq, P. Assessment of potential positive effects of nZVI surface modification and concentration levels on TCE dechlorination in the presence of competing strong oxidants, using an experimental design. *Sci. Total Environ.* **2014**, *481*, 335–342. [CrossRef] [PubMed]

15. Guan, X.H.; Sun, Y.K.; Qin, H.J.; Li, J.X.; Lo, I.M.C.; He, D.; Dong, H.R. The limitations of applying zero-valent iron technology in contaminants sequestration and the corresponding countermeasures: The development in zero-valent iron technology in the last two decades (1994–2014). *Water Res.* **2015**, *75*, 224–248. [CrossRef]
16. Zhao, X.; Liu, W.; Cai, Z.Q.; Han, B.; Qian, T.W.; Zhao, D.Y. An overview of preparation and applications of stabilized zero-valent iron nanoparticles for soil and groundwater remediation. *Water Res.* **2016**, *100*, 245–266. [CrossRef]
17. Kakavandi, B.; Takdastan, A.; Pourfadakari, S.; Ahmadmoazzam, M.; Jorfi, S. Heterogeneous catalytic degradation of organic compounds using nanoscale zero-valent iron supported on kaolinite: Mechanism, kinetic and feasibility studies. *J. Taiwan Inst. Chem. Eng.* **2019**, *96*, 329–340. [CrossRef]
18. Liu, H.; Ruan, X.; Zhao, D.Y.; Fan, X.Y.; Feng, T. Enhanced Adsorption of 2, 4-Dichlorophenol by Nanoscale Zero-Valent Iron Loaded on Bentonite and Modified with a Cationic Surfactant. *Ind. Eng. Chem. Res.* **2016**, *56*, 191–197. [CrossRef]
19. Daraei, H.; Rafiee, M.; Yazdanbakhsh, A.R.; Amoozegar, M.A.; Guanglei, Q. A comparative study on the toxicity of nano zero valent iron (nZVI) on aerobic granular sludge and flocculent activated sludge: Reactor performance, microbial behavior, and mechanism of toxicity. *Process. Saf. Environ.* **2019**, *129*, 238–248. [CrossRef]
20. Mortazavian, S.; An, H.; Chun, D.; Moon, J. Activated carbon impregnated by zero-valent iron nanoparticles (AC/nZVI) optimized for simultaneous adsorption and reduction of aqueous hexavalent chromium: Material characterizations and kinetic studies. *Chem. Eng. J.* **2018**, *353*, 781–795. [CrossRef]
21. Baikousi, M.; Georgiou, Y.; Daikopoulos, C.; Bourlinos, A.B.; Filip, J.; Zbořil, R.; Deligiannakis, Y.; Karakassides, M.A. Synthesis and characterization of robust zero valent iron/mesoporous carbon composites and their applications in arsenic removal. *Carbon* **2015**, *93*, 636–647. [CrossRef]
22. Wan, J.J.; Feng, X.; Li, Y.; He, J.Q.; Zhao, N.; Liu, Z.F.; Lin, Y.J.; Yang, C.X.; Liang, W.Q. Effect of mesoporous silica molecular sieve coating on nZVI for 2, 4-DCP degradation: Morphology and mechanism during the reaction. *Chem. Eng. Process.* **2019**, *135*, 68–81. [CrossRef]
23. Sun, Y.P.; Li, X.Q.; Zhang, W.X.; Wang, H.P. A method for the preparation of stable dispersion of zero-valent iron nanoparticles. *Colloids Surf. Physicochem. Eng.* **2007**, *308*, 60–66. [CrossRef]
24. Yang, J.C.; Wang, X.Y.; Zhu, M.P.; Liu, H.L.; Ma, J. Investigation of PAA/PVDF–NZVI hybrids for metronidazole removal: Synthesis, characterization, and reactivity characteristics. *J. Hazard. Mater.* **2014**, *264*, 269–277. [CrossRef] [PubMed]
25. Alvarado-Gomez, E.; Martínez-Castañon, G.; Sanchez-Sanchez, R.; Ganem-Rondero, A.; Yacaman, M.J.; Martinez-Gutierrez, F. Evaluation of anti-biofilm and cytotoxic effect of a gel formulation with Pluronic F-127 and silver nanoparticles as a potential treatment for skin wounds. *Mater. Sci. Eng. C* **2018**, *92*, 621–630. [CrossRef]
26. Alidokht, L.; Khataee, A.R.; Reyhanitabar, A.; Oustan, S. Cr(VI) Immobilization Process in a Cr-Spiked Soil by Zerovalent Iron Nanoparticles: Optimization Using Response Surface Methodology. *CLEAN Soil Air Water* **2011**, *39*, 633–640. [CrossRef]
27. Rai, P.; Pandey, A.; Pandey, A. Optimization of sugar release from banana peel powder waste (BPPW) using box-behnken design (BBD): BPPW to biohydrogen conversion. *Int. J. Hydrogen Energy* **2019**, *44*, 25505–25513. [CrossRef]
28. Abdulgader, M.; Yu, J.; Zinatizadeh, A.A.; Williams, P.; Rahimi, Z. Process analysis and optimization of single stage flexible fibre biofilm reactor treating milk processing industrial wastewater using response surface methodology (RSM). *Chem. Eng. Res. Des.* **2019**, *149*, 169–181. [CrossRef]
29. Long, X.Y.; Cai, L.C.; Li, W.Z. RSM-based assessment of pavement concrete mechanical properties under joint action of corrosion, fatigue, and fiber content. *Constr. Build. Mater.* **2019**, *197*, 406–420. [CrossRef]
30. Fang, Z.Q.; Qiu, X.Q.; Chen, J.H.; Qiu, X.H. Degradation of metronidazole by nanoscale zero-valent metal prepared from steel pickling waste liquor. *Appl. Catal. B Environ.* **2010**, *100*, 221–228. [CrossRef]
31. Wang, X.Y.; Cong, S.; Wang, P.; Ma, J.; Liu, H.L.; Ning, P. Novel green micelles Pluronic F-127 coating performance on nano zero-valent iron: Enhanced reactivity and innovative kinetics. *Sep. Purif. Technol.* **2017**, *174*, 174–182. [CrossRef]
32. Zhang, X.; Lin, S.; Chen, Z.; Megharaj, M.; Naidu, R. Kaolinite-supported nanoscale zero-valent iron for removal of Pb2+ from aqueous solution: Reactivity, characterization and mechanism. *Water Res.* **2011**, *45*, 3481–3488. [CrossRef] [PubMed]

33. Li, H.Y.; Ge, Y.; Zhang, X.R. High efficient removal of lead from aqueous solution by preparation of novel PPG-nZVI beads as sorbents. *Colloid Surf. A* **2017**, *513*, 306–314. [CrossRef]
34. Iqbal, M.M.A.; Bakar, W.A.W.A.; Toemen, S.; Razak, F.I.A.; Azelee, N.I.W. Optimization study by Box-Behnken design (BBD) and mechanistic insight of CO_2 methanation over Ru-Fe-Ce/γ-Al_2O_3 catalyst by in-situ FTIR technique. *Arab. J. Chem.* **2020**, *13*, 4170–4179. [CrossRef]
35. Liu, J.; Liu, A.R.; Zhang, W.X. The influence of polyelectrolyte modification on nanoscale zero-valent iron (nZVI): Aggregation, sedimentation, and reactivity with Ni (II) in water. *Chem. Eng. J.* **2016**, *303*, 268–274. [CrossRef]
36. Dong, H.R.; Ahmad, K.; Zeng, G.M.; Li, Z.W.; Chen, G.Q.; He, Q.; Xie, Y.K.; Wu, Y.N.; Zhao, F.; Zeng, Y.L. Influence of fulvic acid on the colloidal stability and reactivity of nanoscale zero-valent iron. *Environ. Pollut.* **2016**, *211*, 363–369. [CrossRef]
37. Li, Z.H.; Xu, S.Y.; Xiao, G.H.; Qian, L.M.; Song, Y. Removal of hexavalent chromium from groundwater using sodium alginate dispersed nano zero-valent iron. *J. Environ. Manag.* **2019**, *244*, 33–39. [CrossRef]